16 Feb 2017

Surrogate Modeling of Ultrasonic Simulations using Data-Driven Methods

Xiaosong Du
Missouri University of Science and Technology, xdnwp@mst.edu

Robert Grandin

Leifur Leifsson

Recommended Citation

X. Du et al., "Surrogate Modeling of Ultrasonic Simulations using Data-Driven Methods," *AIP Conference Proceedings*, vol. 1806, article no. 150002, American Institute of Physics, Feb 2017.
The definitive version is available at https://doi.org/10.1063/1.4974726

Surrogate modeling of ultrasonic simulations using data-driven methods

Cite as: AIP Conference Proceedings **1806**, 150002 (2017); https://doi.org/10.1063/1.4974726
Published Online: 16 February 2017

Xiaosong Du, Robert Grandin and Leifur Leifsson

Surrogate Modeling of Ultrasonic Simulations Using Data-Driven Methods

Xiaosong Du[1,a)], Robert Grandin[2,b)], and Leifur Leifsson[1,2,c)]

[1]*Simulation-Driven Optimization Laboratory, Department of Aerospace Engineering, Iowa State University, 537 Bissell Road, Ames IA, 50011, USA*
[2]*Center for Nondestructive Evaluation, Iowa State University, 1915 Scholl Road, Ames IA, 50011, USA*

[a)]Corresponding author: xiaosong@iastate.edu
[b)]rgrandin@iastate.edu
[c)]leifur@iastate.edu

Abstract. Ultrasonic testing (UT) is used to detect internal flaws in materials and to characterize material properties. In many applications, computational simulations are an important part of the inspection-design and analysis processes. Having fast surrogate models for UT simulations is key for enabling efficient inverse analysis and model-assisted probability of detection (MAPOD). In many cases, it is impractical to perform the aforementioned tasks in a timely manner using current simulation models directly. Fast surrogate models can make these processes computationally tractable. This paper presents investigations of using surrogate modeling techniques to create fast approximate models of UT simulator responses. In particular, we propose to integrate data-driven methods (here, kriging interpolation with variable-fidelity models to construct an accurate and fast surrogate model. These techniques are investigated using test cases involving UT simulations of solid components immersed in a water bath during the inspection process. We will apply the full ultrasonic solver and the surrogate model to the detection and characterization of the flaw. The methods will be compared in terms of quality of the responses.

INTRODUCTION

Ultrasonic testing (UT) involves the propagation of high-frequency stress waves through a component [1, 2]. Computational models of varying degrees of fidelity are employed to predict the propagation of the stress wave and generate a synthetic measurement. Predictive measurements such as this are used when designing ultrasonic inspections as well as analyzing experimental data. Utilizing models to analyze experimental data often involves running the predictive models through hundreds, or thousands, of iterations until the collection of input parameters produce a prediction which matches the measurement. Rigorous inversion then requires additional model calculations to evaluate the uniqueness of that solution. Due to this significant computational burden, surrogate models are often needed in order to efficiently explore the parameter space.

In this work, a Kriging surrogate model is applied in place of an actual ultrasonic model. To test the behavior of the Kriging model, five test cases are investigated: steel block, immersion, planar probe; steel block, contact, planar probe; lucite block, contact, planar probe; Lucite block, contact, focused probe; and aluminum block, contact, focused probe. All these results show that the Kriging model works accurately to duplicate the behavior of actual model. Finally, some conclusions are given and future work are mentioned.

SURROGATE MODELING

A surrogate model [3] is a computationally inexpensive mathematical or physical model which replaces the original expensive model. The reduced computational cost enables accelerated simulation and optimization when using the surrogate. To generate appropriate surrogates it is necessary to distribute sample points randomly throughout entire design space and this is typically accomplished through a rigorous Design of Experiment (DoE) [4]. These sample points need to be calculated using the actual model, however the time cost of this sampling is always far less

43rd Annual Review of Progress in Quantitative Nondestructive Evaluation, Volume 36
AIP Conf. Proc. 1806, 150002-1–150002-9; doi: 10.1063/1.4974726
Published by AIP Publishing. 978-0-7354-1474-7/$30.00

than performing optimization via the actual model. This is the key advantage of a surrogate model: leverage a very small number of sample points to generate a surrogate representation of sufficient accuracy which enables efficient optimization.

Generally, surrogate modeling is grouped into two broad categories based on approximation strategy: data-driven [5] and physics-based methods [6]. For data-driven methods, the actual model is treated like a "black box", whose inputs and outputs are the only things to be considered. In contrast, physics-based methods will go through physical nature of problems, but use a simplified low-fidelity model. The final output of a physics-based model is obtained by correcting this low-fidelity model based on using parameters obtained from the high-fidelity model evaluated at the sample points.

In this work Kriging [7] is selected as the surrogate model, because of the nature of the ultrasonic modeling problem. Kriging is a data-driven interpolating method which considers the observed data at all sample points. Kriging provides a statistical prediction of an unknown function by minimizing its Mean Squared Error (MSE). It can be equivalent to any order of polynomials and is thus well suited for a highly-nonlinear function with multiple extremes. Its basic function can be written as the sum of a global trend function, $\mathbf{f}^T(\mathbf{x})\boldsymbol{\beta}$, and a Gaussian random function, Z($\mathbf{x}$), as follows

$$y(\mathbf{x}) = \mathbf{f}^T(\mathbf{x})\boldsymbol{\beta} + Z(\mathbf{x}), \mathbf{x} \in \mathbb{R}^m, \tag{1}$$

where $\mathbf{f}(\mathbf{x}) = [f_0(\mathbf{x}), ..., f_{p-1}(\mathbf{x})]^T \in \mathbb{R}^p$ is defined with a set of the regression basis functions and $\boldsymbol{\beta} = [\beta_0, ..., \beta_{p-1}]^T \in \mathbb{R}^p$ denotes the vector of the corresponding coefficients. In general, $\mathbf{f}^T(\mathbf{x})\boldsymbol{\beta}$ is taken as either a constant or low-order polynomials. Practice suggests that the constant trend function is sufficient for most problems. Thus, $\mathbf{f}^T(\mathbf{x})\boldsymbol{\beta}$ is taken as a constant β_0 in the text hereafter. In Eq. 1, Z($\mathbf{x}$) denotes a stationary random process with zero mean, variance σ^2 and nonzero covariance

$$Cov\left[Z(\mathbf{x}), Z(\mathbf{x'})\right] = \sigma^2 R(\mathbf{x},\mathbf{x'}). \tag{2}$$

Here, R($\mathbf{x}$,$\mathbf{x}$´) is the correlation function which is only dependent on the Euclidean distance between any two sites $\mathbf{x}$ and $\mathbf{x}$´ in the design space. In this study, a Gaussian exponential correlation function is adopted, and it is of the form

$$R(\mathbf{x},\mathbf{x'}) = exp\left[-\sum_{k=1}^{m} \theta_k \left| x_k - x'_k \right|^{p_k}\right], 1 < p_k \leq 2, \tag{3}$$

where $\boldsymbol{\theta} = [\theta_1, \theta_2, ..., \theta_m]^T$ and $\mathbf{p} = [p_1, p_2, ..., p_m]^T$ denote the vectors of the unknown model parameters (hyper parameters) to be tuned.

From the derivation by Sacks [8], the Kriging predictor $\hat{y}$(x) for any untried $\mathbf{x}$ can be written as

$$\hat{y}(\mathbf{x}) = \beta_0 + \mathbf{r}^T(\mathbf{x})\mathbf{R}^{-1}(\mathbf{y}_S - \beta_0\mathbf{1}), \tag{4}$$

where the generalized least square estimation of β_0 is

$$\beta_0 = (\mathbf{1}^T\mathbf{R}^{-1}\mathbf{1})^{-1}\mathbf{1}^T\mathbf{R}^{-1}\mathbf{y}_S, \tag{5}$$

with $\mathbf{1} \in \mathbb{R}^n$ being a vector filled with ones, and **R, r** are the correlation matrix and the correlation vector, respectively. $\mathbf{R}$ and $\mathbf{r}$ are defined as

$$\mathbf{R} = \begin{bmatrix} R(\mathbf{x}^{(1)}, \mathbf{x}^{(1)}) & R(\mathbf{x}^{(1)}, \mathbf{x}^{(2)}) & \cdots & R(\mathbf{x}^{(1)}, \mathbf{x}^{(n)}) \\ R(\mathbf{x}^{(2)}, \mathbf{x}^{(1)}) & R(\mathbf{x}^{(2)}, \mathbf{x}^{(2)}) & \cdots & R(\mathbf{x}^{(2)}, \mathbf{x}^{(n)}) \\ \vdots & \vdots & \ddots & \vdots \\ R(\mathbf{x}^{(n)}, \mathbf{x}^{(1)}) & R(\mathbf{x}^{(n)}, \mathbf{x}^{(2)}) & \cdots & R(\mathbf{x}^{(n)}, \mathbf{x}^{(n)}) \end{bmatrix} \in \mathbb{R}^{n\times n}, \mathbf{r} = \begin{bmatrix} R(\mathbf{x}^(1), \mathbf{x}) \\ R(\mathbf{x}^(2), \mathbf{x}) \\ \vdots \\ R(\mathbf{x}^(n), \mathbf{x}) \end{bmatrix} \in \mathbb{R}^n, \tag{6}$$

where $R(\mathbf{x}^{(i)}, \mathbf{x}^{(j)})$ denotes the correlation between any two observed points $\mathbf{x}^{(i)}$ and $\mathbf{x}^{(j)}$. Similarly, $R(\mathbf{x}^{(i)}, \mathbf{x})$ denotes the correlation between the i-th observed point $\mathbf{x}^{(i)}$ and the untried point $\mathbf{x}$.

A unique feature of Kriging model is that it provides an uncertainty estimation (or MSE) for the prediction, which is very useful for sample-points refinement. This uncertainty estimate has the form

$$\hat{s}(\mathbf{x}) = \sigma^2 \left[1.0 - \mathbf{r}^T \mathbf{R}^{-1} \mathbf{r} + \frac{(\mathbf{r}^T \mathbf{R}^{-1} \mathbf{1} - 1)^2}{\mathbf{1}^T \mathbf{R}^{-1} \mathbf{1}} \right]. \tag{7}$$

Assuming that the sampled data are distributed according tgo a Gaussian process, the responses at sampling sites are considered to be correlated random functions with the corresponding likelihood function given by

$$L(\beta_0, \sigma^2, \boldsymbol{\theta}, \mathbf{p}) = \frac{1}{\sqrt{2\pi(\sigma^2)^n |\mathbf{R}|}} exp\left(-\frac{1}{2} \frac{(\mathbf{y}_S - \beta_0 \mathbf{1})^T \mathbf{R}^{-1} (\mathbf{y}_S - \beta_0 \mathbf{1})}{\sigma^2} \right). \tag{8}$$

The optimal estimation of β_0 and the process variance

$$\beta_0(\boldsymbol{\theta}, \mathbf{p}) = (\mathbf{1}^T \mathbf{R}^{-1} \mathbf{1})^{-1} \mathbf{1}^T \mathbf{R}^{-1} \mathbf{y}_S, \tag{9}$$

$$\sigma^2(\beta_0, \theta, p) = \frac{1}{n} (\mathbf{y}_S - \beta_0 \mathbf{1})^T \mathbf{R}^{-1} (\mathbf{y}_S - \beta_0 \mathbf{1}) \tag{10}$$

are obtained analytically, yet depend on the remaining hyper-parameters $\boldsymbol{\theta} = [\theta_1, \theta_2, ..., \theta_m]^T$ and $\mathbf{p} = [p_1, p_2, ..., p_m]^T$. Substituting it into the associated Equation and taking the logarithm, we are left with maximizing

$$MLE(\boldsymbol{\theta}, \mathbf{p}) = -n \ln \sigma^2(\boldsymbol{\theta}) - \ln |\mathbf{R}(\boldsymbol{\theta})|, \tag{11}$$

which can be solved through numerical methods such as a Genetic Algorithm [9].

ULTRASONIC MODEL

Ultrasonic simulation capability is provided using a Gauss-Hermite beam model [10], which models the ultrasonic beam using a collection of Gaussian-weighted Hermite polynomials coupled with the paraxial approximation. This formulation supports fast calculations and provides applicability to many industrially-relevant inspections. The model is implemented within UTSim2, a new ultrasonic simulation platform recently developed at Iowa State's Center for Nondestructive Evaluation [11].

For the purposes of this investigation, the beam model is utilized to predict the strength of the incident ultrasonic field within the solid. The model implementation utilizes a modified form the Thompson-Gray measurement model [1] which only considers the system efficiency factor, β, and forward beam propagation:

$$d\Gamma(\omega) = \beta(\omega) \left[TC(\omega) P(\omega) \right], \tag{12}$$

where, ω: Frequency, expressed in radians per second, $d\Gamma$: Complex-valued spectrum of the incident field, β: Complex-valued system efficiency factor, which captures the spectral characteristics of the pulser/receiver, cabling, and transducer, T: Real-valued fluid-solid transmission coefficient, C: Complex-valued beam diffraction correction, P: Complex-valued beam propagation and attenuation.Reflection from a small flaw, which is part of the standard Thompson-Gray measurement model, is not considered since the the surrogate model only considers the UT beam which is independent from the flaw scattering in the Thompson-Gray formulation.

Due to $d\Gamma$ representing the spectrum of a real-valued voltage signal, Eq. (12) is only evaluated for positive frequencies and the negative frequencies are defined to be conjugate-symmetric. An example of the volumetric beam amplitude is shown in Fig. 2(a).

Model Setup and Outputs

For this investigation, a simple simulation setup is considered, in which a rectangular solid is immersed within a water bath. The fluid-solid interface is planar and the transducer is oriented normal to this interface. The simulation geometry is shown in Fig. 1.

As part of this investigation the effects of varying key parameters was explored

- Contact vs. non-contact transducer position
- Focused vs. unfocused transducer
- Solid material properties, including lucite, steel, and aluminum

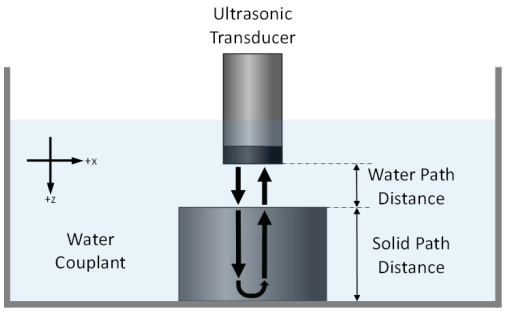

FIGURE 1. Simulation geometry, showing the solid immersed in water with a planar fluid-solid interface.

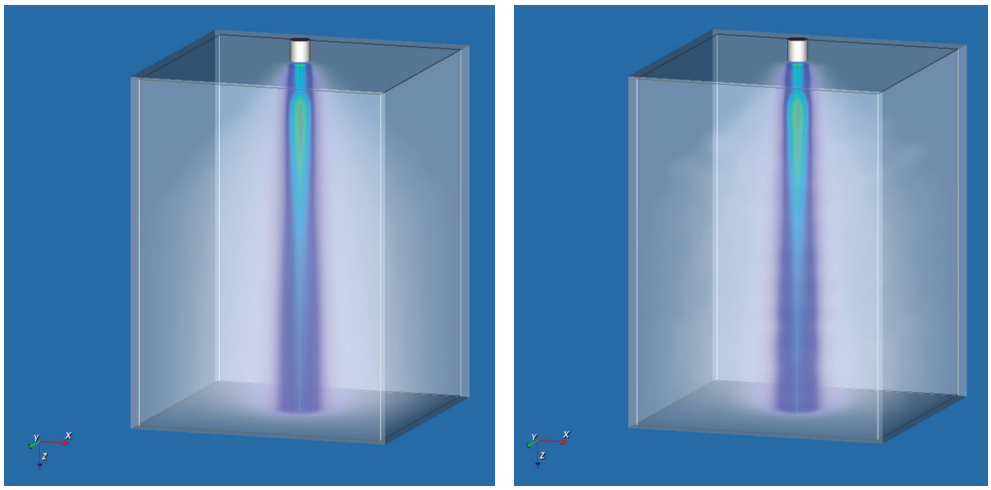

(a) Incident field, Gauss-Hermite model (b) Incident field, surrogate model

FIGURE 2. Incident field calculation results for both the Gauss-Hermite model and the surrogate model

Within the context of the measurement model (Eq. (12)), the Gauss-Hermite beam model calculates the quantity $[TC(\omega)P(\omega)]$, including the effects of interface curvature and the material properties of the fluid and solid. The product of these terms can be thought of as complex-valued ultrasonic particle displacement spectrum, $D(\omega)$. It is this spectrum, $D(\omega)$, which is modeled by the surrogate. This leads to the consideration of two output quantities when evaluating the quality of the surrogate model.

First, the maximum displacement is considered at each point in the simulation volume. This produces the volumetric results seen in Fig. 2. Mathematically,

$$A(x,y,z) = max\left[\mathscr{F}^{-1}(D(\omega,x,y,z)\right], \tag{13}$$

where $\mathscr{F}^{-1}$ denotes the inverse Fourier Transform. This provides a comparison which closely resembles quantities which may be measured experimentally. A qualitative volumetric comparison is shown in Fig. 2.

The second analysis involves directly comparing $D(\omega)_{Gauss-Hermite}$ to $D(\omega)_{Surrogate}$ and will be discussed in the following section.

NUMERICAL RESULTS

In this section 5 test cases are considered for validation. The test cases include:

- Steel block, immersion, planar probe

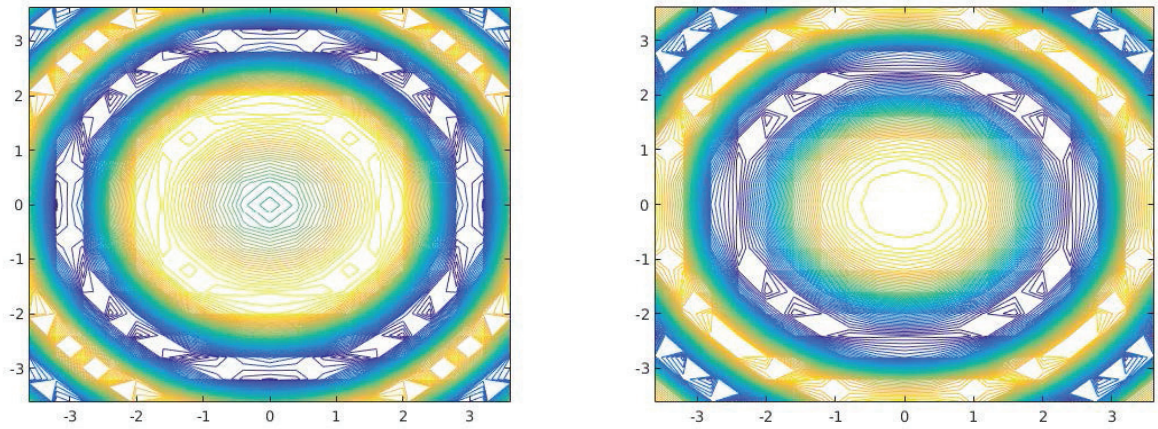

FIGURE 3. Symmetry in one z-coordinate slice (left: real part of computed value; right: imagine part of computed value)

- Steel block, contact, planar probe
- Lucite block, contact, planar probe
- Lucite block, contact, focused probe
- Aluminum block, contact, focused probe

For each test case the block surface is planar and the transducer is oriented normal to the water-solid interface. This orientation produces symmetrical beam properties about the propagation axis, as shown in Fig. 3.

This symmetry allows simplifying the computation since only a quarter of the beam must be calculated. In the following part, all test cases will be mentioned for surrogate model construction. For each test case, the number of data points in the original calculation will be given along with the size of the subset which was used to build the surrogate model. Each row of data contains the $(x, y, z, \omega, d_{real}, d_{imag})$ values associated with a calculation point.

Test Case 1: Steel Block, Immersion, Planar Probe

In this case, the total data will be reduced from 1,541,200 to 343,000 rows, after symmetry simplification. To generate the surrogate model, 14,472 rows of data are selected as sample points. The number of sample points is selected for accuracy and efficiency of Kriging model. To validate the model, root mean squared error (RMSE) is tested as Table 1. The plot is also shown in Fig. 4

In Table 1, the RMSE of both d_{real} and d_{imag} drops greatly with the increased number of sample points. In surrogate modeling a model is considered sufficiently good once the RMSE drops below the standard deviation of the sampled data [12]. In this test case, that corresponds to the model generated from the 14,472 sample points.

Test Case 2: Steel Block, Contact, Planar Probe

In this case, the total data will be reduced from 1,406,800 to 312,200 rows, after symmetry simplification. To generate the surrogate model, 12,828 rows of data are selected as sample points. Validation results are shown in Table 2 and Fig. 5

Here, significantly fewer sample points may be selected to satisfy the requirement that RMSE is kept below the standard deviation. However, it is shown that significant accuracy gains are achieved through a model developed with additional sampling.

Test Case 3: Lucite Block, Contact, Planar Probe

In this case, the total data will be reduced from 877,200 to 189,600 rows, after symmetry simplification. To generate the surrogate model, 7,992 rows of data are selected as sample points. Validation results for this scenario are shown in Table 3 and Fig. 6

In this case, the standard deviation is rather large, so it is easy to achieve sufficiently-small enough RMSE.

Test Case 4: Lucite Block, Contact, Focused Probe

In this case, the total data will be reduced from 886,800 to 253,200 rows, after symmetry simplification. To generate the surrogate model, 7,620 rows of data are selected as sample points. Validation results are shown in Table 4 and Fig. 7

Again, the large variance of the sample data allows a suitable model to be developed from a small collection of sample points.

Test Case 5: Aluminum Block, Contact, Focused Probe

In this final case, the total data will be reduced from 1,440,400 to 402,000 rows, after symmetry simplification. To generate the surrogate model, 13,344 rows of data are selected as sample points. Validation results are shown in Table 5 and Fig. 8.

Unlike cases 3 and 4, much larger sample sets are required to generate a suitable surrogate model due to the significantly smaller variance of the sample data.

TABLE 1. RMSE for test case 1.

	d_{real}		d_{imag}	
No. Sample Pts.	**RMSE**	**Std. Dev.**	**RMSE**	**Std. Dev.**
226	4.47%	2.93%	4.53%	3.17%
904	4.19%	2.93%	4.17%	3.17%
3618	4.08%	2.93%	3.26%	3.17%
14472	1.91%	2.93%	2.10%	3.17%

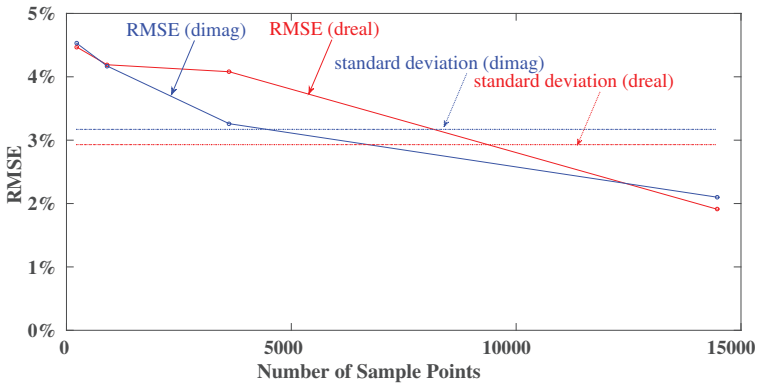

FIGURE 4. Plots of RMSE versus the number of sample points in test case 1

TABLE 2. RMSE for test case 2.

	d_{real}		d_{imag}	
No. Sample Pts.	**RMSE**	**Std. Dev.**	**RMSE**	**Std. Dev.**
200	10.79%	12.35%	11.13%	10.96%
801	10.03%	12.35%	10.76%	10.96%
3207	5.18%	12.35%	5.96%	10.96%
12828	1.96%	12.35%	2.06%	10.96%

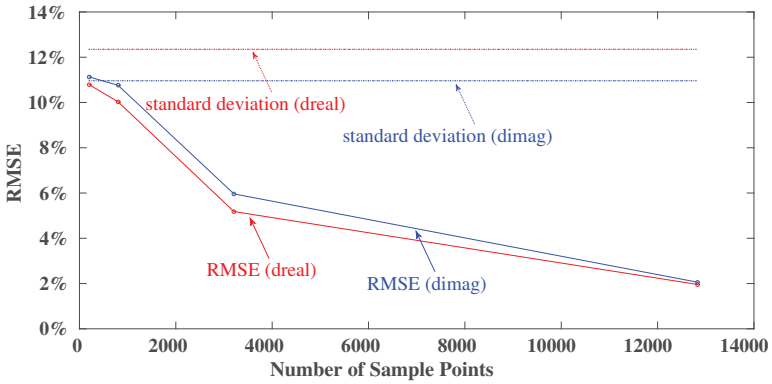

FIGURE 5. Plots of RMSE versus the number of sample points in test case 2

TABLE 3. RMSE for test case 3.

	d_{real}		d_{imag}	
No. Sample Pts.	**RMSE**	**Std. Dev.**	**RMSE**	**Std. Dev.**
124	7.18%	9.93%	14.05%	12.92%
499	5.84%	9.93%	5.68%	12.92%
1998	3.86%	9.93%	4.47%	12.92%
7992	2.16%	9.93%	2.21%	12.92%

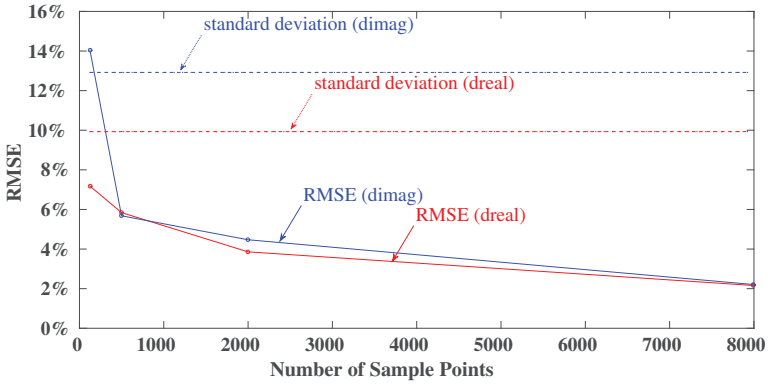

FIGURE 6. Plots of RMSE versus the number of sample points in test case 3

TABLE 4. RMSE for test case 4.

	d_{real}		d_{imag}	
No. Sample Pts.	**RMSE**	**Std. Dev.**	**RMSE**	**Std. Dev.**
119	10.59%	19.56%	16.55%	14.66%
476	8.70%	19.56%	15.26%	14.66%
1905	7.04%	19.56%	13.29%	14.66%
7620	2.42%	19.56%	2.59%	14.66%

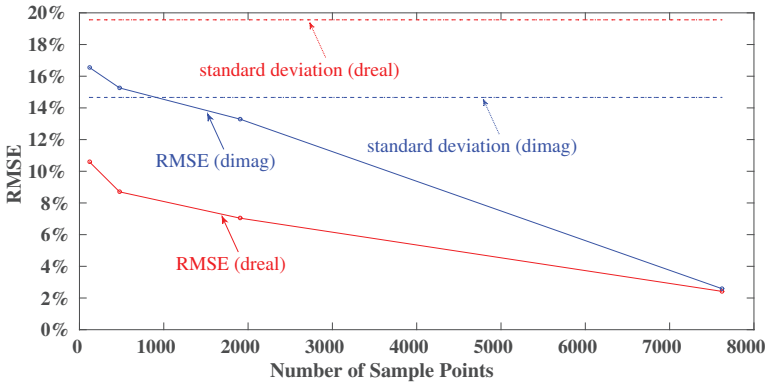

FIGURE 7. Plots of RMSE versus the number of sample points in test case 4

TABLE 5. RMSE for test case 5.

	d_{real}		d_{imag}	
No. Sample Pts.	**RMSE**	**Std. Dev.**	**RMSE**	**Std. Dev.**
208	5.96%	3.00%	6.05%	4.63%
834	4.26%	3.00%	5.68%	4.63%
3336	3.38%	3.00%	4.44%	4.63%
13344	3.19%	3.00%	4.13%	4.63%

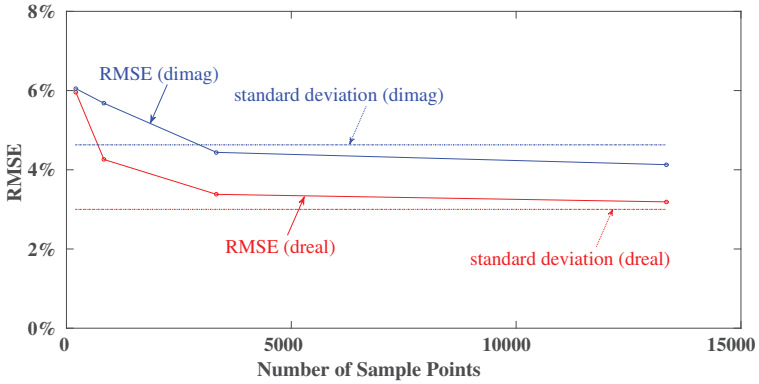

FIGURE 8. Plots of RMSE versus the number of sample points in test case 5

SUMMARY AND FUTURE WORK

The results presented here demonstrate the applicability of Kriging interpolation to modeling UT beam intensities. The selected test cases show that a suitable model may be developed so long as adequate sampling is provided. Future work will need to consider the computational performance of the surrogate as well as further-explore parameter spaces associated with common UT inspections. Additionally, the applicability of the Kriging model to model-assisted probability of detection (MAPOD) will need to be explored due to the need for accelerated computational approaches in MAPOD activities.

Future work will seek to improve Kriging model in the following ways: 1. $D(\omega, x, y, z)$ reflects symmetries associated with the transducer geometry, allowing a reduction of input variables. For the circular transducers considered here (x, y) coordinates can simply be reduced to a radial position, r. Simplifications such as this greatly reduce the size of the Kriging model and accelerate its evaluation. 2. The Kriging methodology itself has many improved versions, such as co-Kriging [13], which applies a multi-grid approach to the Kriging implementation. In future work, a very coarse Kriging model can be leveraged as the basic function, while a fine Kriging model is utilized to correct the final response. This will provide further computational acceleration.

REFERENCES

1. R. B. Thompson and T. A. Gray, A model relating ultrasonic scattering measurements through liquid solid interfaces to unbounded medium scattering amplitudes, JASA **74**, 1279–1290 (1983).
2. R. Roberts, Phased Array Beam Modeling Using a Discretely Orthogonal Gaussian Aperture Basis, AIP Conference Proceedings **700**, 785–792 (2004).
3. S. Koziel and L. Leifsson, in *Simulation-Driven Design by Knowledge-Based Response Correction Techniques* (Springer, 2016), pp. 31–60.
4. D. Cox and N. Reid, in *The Theory of the Design of Experiments* (Chapman and Hall/CRC, 2000).
5. S. Deshpande, L. T. Watson, J. Shu, F. A. Kamke, and N. Ramakrishnan, Data driven surrogate-based optimization in the problem solving environment WBCSim, Engineering with Computers (2010), 10.1007/s00366-010-0192-8.
6. L. Leifsson and S. Koziel, Multi-fidelity design optimization of transonic airfoils using physics-based surrogate modeling and shape-preserving response prediction, Journal of Computational Science **2** (1) 98–106 (2010).
7. M. Shahbaz, Z. Han, J. Liu, and W. Song, An Efficient Robust Aerodynamic Design Optimization under Aleatory Uncertainty, International Conference on Innovative Engineering Technologies (ICIET2014) 102–109 (2014).
8. J. Sacks, W. J. Welch, T. J. Mitchell, and H. P. Wynn, Design and Analysis of Computer Experiments, Statistical Science **4**, 409–423 (1989).
9. O. Roeva, in *Surrogate-Based Optimization, Real-World Applications of Genetic Algorithms* (InTech, 2012), pp. 318–343.
10. B. Cook and W. I. Arnoult, Gaussian-Laguerre/Hermite formulation for the nearfield of an ultrasonic transducer, JASA **59**, 9–11 (1976).
11. R. Grandin and T. Gray, "UTSim2 Validation," in *These Proceedings* (2017).
12. A. I. J. Forrester, A. Sobester, and A. J. Keane, in *Engineering Design via Surrogate Modelling: A Practical Guide* (John Wiley and Sons, Ltd., 2008), pp. 33–76.
13. S. Koziel, L. Leifsson, I. Couckuyt, and T. Dhaene, Robust variable-fidelity optimization of microwave filters using co-kriging and trust regions, Microwave and Optical Technology Letter **55**, 765–769 (2013).